Spatial dependence of output pulse delay in a niobium nitride nanowire superconducting single-photon detector

J. A. O'Connor, M. G. Tanner, C. M. Natarajan, G. S. Buller, R. J. Warburton, S. Miki, Z. Wang, S. W. Nam, and R. H. Hadfield

Articles you may be interested in

Optical time domain reflectometry with low noise waveguide-coupled superconducting nanowire single-photon detectors
Appl. Phys. Lett. **102**, 191104 (2013); 10.1063/1.4803011

NbTiN superconducting nanowire detectors for visible and telecom wavelengths single photon counting on Si3N4 photonic circuits
Appl. Phys. Lett. **102**, 051101 (2013); 10.1063/1.4788931

Broadening of hot-spot response spectrum of superconducting NbN nanowire single-photon detector with reduced nitrogen content
J. Appl. Phys. **112**, 074511 (2012); 10.1063/1.4757625

Nanowire superconducting single-photon detectors on GaAs for integrated quantum photonic applications
Appl. Phys. Lett. **97**, 151108 (2010); 10.1063/1.3496457

Intrinsic detection efficiency of superconducting nanowire single-photon detectors with different thicknesses
J. Appl. Phys. **108**, 014507 (2010); 10.1063/1.3437043

Spatial dependence of output pulse delay in a niobium nitride nanowire superconducting single-photon detector

J. A. O'Connor,[1] M. G. Tanner,[1] C. M. Natarajan,[1] G. S. Buller,[1] R. J. Warburton,[1,2] S. Miki,[3] Z. Wang,[3] S. W. Nam,[4] and R. H. Hadfield[1,a]

[1]*Scottish Universities Physics Alliance and the School of Engineering and Physical Sciences, Heriot-Watt University, Edinburgh EH14 4AS, United Kingdom*

[2]*Department of Physics, University of Basel, Klingelbergstrasse 82, CH-4056 Basel, Switzerland*

[3]*Kansai Advanced Research Center, National Institute of Information and Communications Technology (NICT), 588-2, Iwaoka, Iwako-cho, Nishi-ku, Kobe, Hyogo 651-2492, Japan*

[4]*National Institute of Standards and Technology, 325 Broadway, Boulder, Colorado 80305, USA*

We report on the position-dependent variation in output pulse timing across a superconducting single-photon detector. Our device consists of a single niobium nitride nanowire meander (100 nm width, 4 nm film thickness, 2 mm length). We use a confocal microscope configuration (full width at half maximum-spot size 1.3 μm at 1550 nm wavelength) and a femtosecond laser to study local variations in detection efficiency and output pulse timing. Pulse delays of up to 50 ps across the device correlate to local detection efficiency and resistance variations. This study indicates an underlying mechanism for timing jitter in superconducting nanowire devices. © *2011 American Institute of Physics*. [doi:10.1063/1.3581054]

Superconducting single-photon detectors (SSPDs) based upon superconducting nanowires[1] have emerged as an important low-noise, high-speed single-photon counting technology for infrared wavelengths. The basic device consists of a 100 nm width nanowire patterned in an ultrathin niobium nitride superconducting thin film. In operation, the device is cooled below its critical temperature and current biased. The absorption of a photon creates a resistive hotspot, triggering a fast voltage pulse that can be amplified and registered by room-temperature timing electronics. To allow efficient optical coupling, the nanowire is folded into a meander geometry to cover a 10 μm$\times$10 μm^2 or 20 μm$\times$20 μm area.[3] Nanowire SSPDs have been used successfully in applications including quantum key distribution,[4–6] quantum information processing,[7] quantum emitter characterization,[8] single-photon time-of-flight ranging,[9] and high-speed communications.[10]

Nano-optical techniques such as confocal microscopy (commonly used in applications such as spectroscopy of semiconductor quantum dots and single molecules) provide a powerful tool for studying SSPD device physics. Previous nano-optical studies include mapping the local detection efficiency of nanowire SSPDs,[11] or studying the spatial resolution of novel SSPD designs.[12] Our previous studies utilized a confocal microscope configuration to focus light onto a device[11] and showed the location of a constriction on a nanowire meander SSPD, by studying the variation in count rate across the device at constant photon flux. This experimental configuration relied on the use of liquid cryogens, which limited the measurement time. A window to room temperature provided optical coupling—in spite of cold filtering, black body heating increased the operating temperature and the dark-count rate. To overcome these problems, for our current study we have constructed a fiber-based miniature confocal microscope[13] integrated in a closed-cycle Gifford

McMahon (GM) refrigerator operating at T$\sim$3 K (illustrated in Fig. 1). To make sample exchange easier, movable optics and a fixed sample were chosen. The simple two-lens optics system is mounted in a titanium holder that is affixed to a stack of slip-stick piezoelectric linear positioners. This gives an overall translation distance of 5 mm in each axis that is used for positioning and focusing of the optics. The doublet lens system design is simple: a collimating aspheric lens (f=11 mm, clear aperture 5.5 mm) with numerical aperture (NA) of 0.25 is chosen to give a close match to both
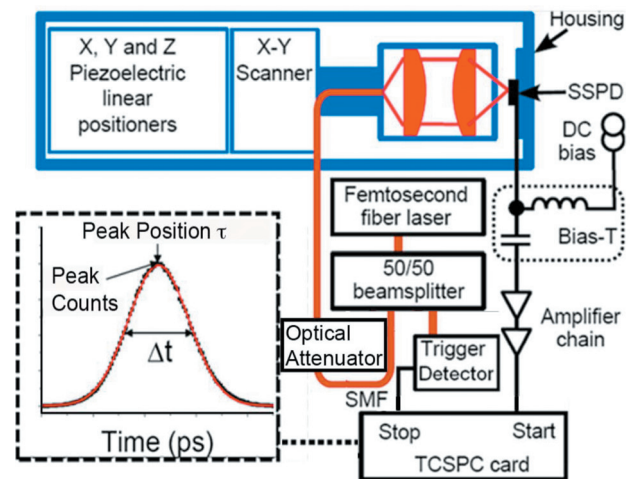

FIG. 1. (Color) Miniature confocal microscope configuration. This allows high resolution scanning over a 30$\times$30 μm^2 area, allowing detection efficiency and instrument response histograms (inset) to be recorded. TCSPC: time-correlated single photon counting card; SSPD: superconducting single-photon detector; SMF: single-mode fiber. Femtosecond fiber laser: λ=1550 nm with 2 mW output power and 50 MHz repetition rate. The SSPD is mounted upside down on the microscope housing, to provide a thermal link for cooling to $\sim$3 K. The trigger detector was a second (fiber-coupled) SSPD for the maps (Fig. 2), and an InGaAs PIN diode for the pulse shapes (Fig. 3). The amplifier chain consists of 580 MHz and 1 GHz bandwidth room-temperature amplifiers. Inset: a typical TCSPC instrument response histogram. A Gaussian fit (solid line) gives the relative timing delay, τ (from the peak position) and the full-width at half maximum timing jitter, Δt.

[a]Electronic mail: r.h.hadfield@hw.ac.uk.

the NA of the optical fiber (0.13) and the clear aperture of the objective aspheric lens (f=2.75 mm, clear aperture 3.6 mm), while permitting a large objective NA (0.68). The end of an optical fiber is secured to the lens housing at a fixed position that collimates the beam when it emerges from the collimating lens. This optical system gives efficient coupling to the sample with high spatial resolution. A piezoelectric x-y scanner provides precision movement across the nanowire SSPD, covering a 30 μm $\times$ 30 μm area with subnanometer resolution. The housing that contains the whole miniature confocal microscope is tightly secured to the GM cold head. Sparrow's criterion[14] gives the expected resolution in the case of an incident plane wave, predicting a full width at half maximum (FWHM) spot of 1185 nm (λ=1550 nm). We determine the FWHM spot by measuring the reflected signal across the edge of gold checkerboard sample and making a Gaussian fit to the differential profile. With no vibrations present, the measured FWHM spot is 1090 $\pm$ 120 nm; with the GM cold head switched on, the measured FWHM spot is 1300 $\pm$ 360 nm. This FWHM spot is significantly smaller than the dimensions of the meander SSPD (20 μm $\times$ 20 μm), meaning that localized parts of the device can be probed (the nanowire width itself is 100 nm with 200 nm pitch, so multiple adjacent segments of the meander are illuminated).

Our aim in this study was to systematically investigate local variations in detection efficiency, timing jitter (Δt) and pulse triggering delay (τ) across a large-area meander device. A 1550 nm femtosecond fiber laser source (output power 2 mW, repetition rate 50 MHz) was used in these measurements. Part of the signal was attenuated to a single-photon level via a calibrated programmable optical attenuator and directed to the SSPD under test in the miniature confocal microscope; the remainder of the signal was sent to a second "trigger" detector. The mean photon flux incident on the SSPD under test was typically ~1 photon per pulse for the measurements shown (although we verified the robustness of the main effects observed by varying the flux from 0.01 to 10 photons per pulse). The electrical output from the SSPD under test is amplified at room temperature (by a 580 MHz and 1 GHz bandwidth low-noise amplifier chain) and used to trigger the "start" channel of a time-correlated single-photon counting (TCSPC) card with 4 ps time bins. Typical output pulse rates were below 10 kHz, owing to the low local detection efficiency of the SSPD under test. The purpose of the trigger detector was to provide a "stop" signal to the TCSPC card on each clock cycle. In the case of the mapping data (Fig. 2), a fiber-coupled SSPD (130 ps FWHM jitter), was used as the "clock" detector, giving an overall $\Delta t \sim 190$ ps; for the pulse shape data [Fig. 3(b)] an InGaAs PIN diode (16 ps FWHM jitter) was used, giving $\Delta t \sim 140$ ps.

For these studies we selected an SSPD meander device with the following characteristics: 100 nm line width, 200 nm pitch, and 20 $\times$ 20 μm^2 area.[3] The nanowire was fabricated using electron beam lithography, using high resolution positive resist, followed by reactive ion etching. At 3 K the measured critical current I_c=12 μA with a (fiber-coupled) detection efficiency of 0.01% at 1550 nm and 1 kHz dark count rate. A uniformity characteristic[15] C=0.35 was obtained from inductance measurements. In comparison to other devices in the same batch,[3] this device had a con-
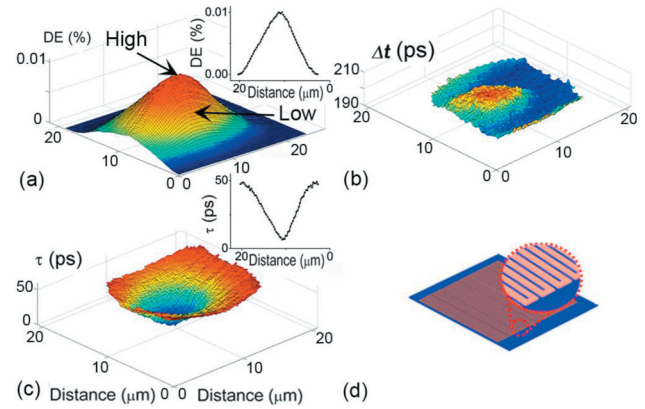

FIG. 2. (Color) Photoresponse maps with timing information across the SSPD obtained via a TCSPC measurement, using a second fiber-coupled SSPD (140 ps FWHM) as trigger. The high and low sensitivity regions of the device are marked. (a) Detection efficiency (DE) map. The maximum DE (0.01%) is observed at the center of the device. As indicated by the insets (taken along a single line across the device through the center) the maximum DE corresponds to the lowest timing delay in (c). (b) Map of FWHM timing jitter Δt (varying between 190 and 205 ps across the device), determined from a Gaussian fit to the histogram at each position [examples of raw data shown in Fig. 3(b)]. (c) Map of output pulse arrival delay, τ, determined from a Gaussian fit to the instrument response function at each point. The maximum variation in τ across the device is 50 ps. (d) SSPD scale schematic, (100 nm width, 200 nm period, 4 nm thickness, 2 mm length, 20 μm $\times$ 20 μm area), with close-up of nanowire structure.

stricted region.[15] The constricted (lowest superconducting cross-section) parts of the nanowire will have the highest current density and the highest relative detection efficiency. The critical current will be limited by constrictions. In our study, we specifically selected this device to give a *variation* in properties across the device area.

Figure 2 shows maps of the following: (a) local detection efficiency measured at constant photon flux; (b) the FWHM timing jitter, Δt [at each point the acquisition time was set to accumulate equal peak counts in the histogram (5000 peak counts and 4 ps time bins) at each position to ensure a consistent Gaussian fit]; (c) the relative pulse arrival delay τ determined from the fitted peak position of the timing jitter histogram; (d) a schematic of the device layout, relative to the preceding plots, showing the orientation of the meander (with magnified close-up of nanowires). Figure 2(a) shows that the central region of the device has the highest efficiency (0.01%) and therefore the highest density of active constrictions. The FWHM diameter of the responsive region
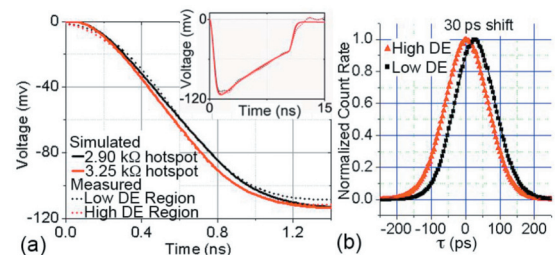

FIG. 3. (Color) (a) Leading edge of output pulses (averaged over 256 shots on an 8 GHz bandwidth oscilloscope) at both high (red solid line) and low (black solid line) sensitivity spots on the device [identified from Fig. 2(a)]. The dashed lines are the simulated pulses (PSPICE model). Inset: full pulse shapes. (b) Instrument response function histogram data (using a TCSPC card and InGaAs PIN diode with 16 ps FWHM jitter as trigger) at the high efficiency spot (Δt=147 ps, red line) and low efficiency spot (Δt=140 ps, black line). The relative timing delay between the peak positions is 30 ps

is much wider than the spot diameter (8.9 μm diameter compared to 1.3 μm spot size). A broad constricted region could arise due to imperfect proximity effect correction during the electron beam exposure on this particular device. Figure 2(b) shows a relatively small variation in Δt across the device (190 ± 5 ps, comparable to the bin size of the timing card). The maximum Δt corresponds to the most sensitive region of the device, where the majority of the active constrictions are located. We believe the slight broadening of Δt occurs in this region as more constrictions are being illuminated simultaneously. Figure 2(c) shows much larger variation in τ across the device area. The central, most sensitive region of the device responds up to 50 ps sooner than the low-efficiency fringes. The measured variation in τ is present even if the device regions are illuminated with different photon fluxes to trigger the same number of counts for each region. This confirms that the observed variation in τ is not an artifact of our experimental setup.

These observations led us to consider whether variations in τ reflect a variation in the detector output pulse leading edge, depending on which part of the SSPD is illuminated. At first sight this would appear unlikely: our amplifier chain has relatively low bandwidth (our initial amplifier had a 3 dB roll off at 580 MHz). However, careful measurements of averaged leading edge pulse shapes (averaged over 256 shots on a 8 GHz bandwidth oscilloscope) from high- and low-sensitivity regions of the device show a distinct variation in rise time [Fig. 3(a)]. In a simple (but highly effective) phenomenological circuit model of the device,[16,17] the time constant of the leading edge of the pulse is given by $L/R_{hotspot}$ (where L is the overall inductance and $R_{hotspot}$ is the hotspot resistance). A PSPICE simulation based on this circuit model shows that a small variation in $R_{hotspot}$ (2.9 kΩ for the low-sensitivity part of the SSPD; 3.25 kΩ for the high-sensitivity part of the SSPD—a difference of just 12%) *should* give rise to a $\tau \sim 30$ ps between the output pulses, even after low-pass filtering via the amplifier chain [Fig. 3(a)].[18] In our measurement setup, the pulses are fed to a TCSPC card with differentiating constant fraction discriminator (CFD). Figure 3(b) shows the measured timing jitter (Δt) histograms for the high- and low-sensitivity regions of the device, with a clear shift of 30 ps between the peak positions. The variation in $R_{hotspot}$ is likely to correspond to slight variations in film quality or cross-sectional area along the 2 mm length of the nanowire. $R_{hotspot}$ from the pulse fit in Fig. 3(a) represents the mean resistance of active constrictions in the illuminated region of the device. The measured Δt [Fig. 3(b)] represents the *spread* in hotspot resistances for active constrictions within the illuminated region. Minimizing Δt in SSPDs is undoubtedly a major point of interest for the research field.[19] Our conclusions support the hypothesis that a nanowire of uniform cross-section will give low Δt, because $R_{hotspot}$ is fixed along the whole wire length. We have observed Δt as low as 60 ps FWHM in the highest efficiency (and therefore most uniform) SSPDs of this design.[7,20]

In conclusion, our nano-optical studies of pulse delay (τ) across a 20 μm $\times$ 20 μm area, 2 mm length nanowire SSPD device show a measurable change in pulse arrival time (up to 50 ps) from high- and low-sensitivity parts of the device.

This is an important step forward in understanding SSPD device physics, indicating why nonuniform nanowires give poor timing jitter. This study has been carried out at a single wavelength ($\lambda = 1550$ nm). In future we intend to investigate whether $R_{hotspot}$ varies with photon energy and whether spectral or photon number information can be extracted by use of the same effect. We also intend to explore (via next generation device designs) whether the observed timing delays can be exploited to extract spatial information with sufficient timing resolution for use in practical applications such as imaging, without compromising other key performance parameters such as device efficiency.

[1]G. N. Gol'tsman, O. Okunev, G. Chulkova, A. Lipatov, A. Semenov, K. Smirnov, B. Voronov, A. Dzardanov, C. Williams, and R. Sobolewski, Appl. Phys. Lett. **79**, 705 (2001).

[2]A. Verevkin, J. Zhang, R. Sobolewski, A. Lipatov, O. Okunev, G. Chulkova, A. Korneev, K. Smirov, G. N. Gol'tsman, and A. Semenov, Appl. Phys. Lett. **80**, 4687 (2002).

[3]S. Miki, M. Fujiwara, M. Sasaki, B. Baek, A. J. Miller, R. H. Hadfield, S. W. Nam, and Z. Wang, Appl. Phys. Lett. **92**, 061116 (2008).

[4]R. H. Hadfield, J. L. Habif, J. Schlafer, R. E. Schwall, and S. Nam, Appl. Phys. Lett. **89**, 241129 (2006).

[5]R. J. Collins, R. H. Hadfield, V. Fernandez, S. W. Nam, and G. S. Buller, Electron. Lett. **43**, 180 (2007).

[6]H. Takesue, S. Nam, Q. Zhang, R. H. Hadfield, T. Honjo, K. Tamaki, and Y. Yamamoto, Nat. Photonics **1**, 343 (2007).

[7]C. M. Natarajan, A. Peruzzo, S. Miki, M. Sasaki, Z. Wang, B. Baek, S. W. Nam, R. H. Hadfield, and J. L. O'Brien, Appl. Phys. Lett. **96**, 211101 (2010).

[8]R. H. Hadfield, M. J. Stevens, S. S. Gruber, A. J. Miller, R. E. Schwall, R. P. Mirin, and S. W. Nam, Opt. Express **13**, 10846 (2005).

[9]R. E. Warburton, A. McCarthy, A. Walker, S. Hernandez-Marin, R. H. Hadfield, S. Nam, and G. S. Buller, Opt. Lett. **32**, 2266 (2007).

[10]B. S. Robinson, A. J. Kerman, E. A. Dauler, R. O. Barron, D. O. Caplan, M. L. Stevens, J. J. Carney, S. A. Hamilton, J. K. W. Yang, and K. K. Berggren, Opt. Lett. **31**, 444 (2006).

[11]R. H. Hadfield, P. A. Dalgarno, J. A. O'Connor, E. Ramsay, R. J. Warburton, E. J. Gansen, B. Baek, M. J. Stevens, R. P. Mirin, and S. W. Nam, Appl. Phys. Lett. **91**, 241108 (2007).

[12]D. Bitauld, F. Marsili, A. Gaggero, F. Mattioli, R. Leoni, S. J. Nejad, F. Levy, and A. Fiore, Nano Lett. **10**, 2977 (2010).

[13]A. Högele, S. Seidl, M. Kroner, K. Karrai, C. Schulhauser, O. Sqalli, J. Scrimgeour, and R. J. Warburton, Rev. Sci. Instrum. **79**, 023709 (2008).

[14]C. M. Sparrow, Astrophys. J. **44**, 76 (1916).

[15]A. J. Kerman, E. A. Dauler, J. K. W. Yang, K. M. Rosfjord, V. Anant, K. K. Berggren, G. N. Gol'tsman, and B. M. Voronov, Appl. Phys. Lett. **90**, 101110 (2007).

[16]A. J. Kerman, E. A. Dauler, W. E. Keicher, J. K. W. Yang, K. K. Berggren, G. Gol'tsman, and B. Voronov, Appl. Phys. Lett. **88**, 111116 (2006).

[17]R. H. Hadfield, A. J. Miller, S. W. Nam, R. L. Kautz, and R. E. Schwall, Appl. Phys. Lett. **87**, 203505 (2005).

[18]Note that in our model we have assumed a time-invariant hotspot resistance, $R_{hotspot}$, instead of a rapidly evolving hotspot resistance $R_{hotspot}(t)$ as presented in J. K. W. Yang, A. J. Kerman, E. A. Dauler, V. Anant, K. M. Rosfjord, and K. K. Berggren, IEEE Trans. Appl. Supercond. **17**, 581 (2007).

[19]R. H. Hadfield, Nat. Photonics **3**, 696 (2009).

[20]C. M. Natarajan, M. M. Häertig, R. E. Warburton, G. S. Buller, R. H. Hadfield, B. Baek, S. W. Nam, S. Miki, M. Fujiwara, M. Sasaki, and Z. Wang, *Quantum Communication and Quantum Networking, Lecture Notes of the Institute for Computer Sciences, Social Informatics, and Telecommunications Engineering* (Springer, Berlin, 2010), 36, Part 3, 225–232.